JTTEE5 17:564–573
DOI: 10.1007/s11666-008-9211-3
1059-9630/$19.00 © ASM International

Particles Spreading Phenomena in the Case of Glass Thermal Spraying

Thierry Poirier, Marie Pierre Planche, Olivier Landemarre, and Christian Coddet

(Submitted October 24, 2007; in revised form January 31, 2008)

The spreading phenomena of particles during thermal spraying are quite difficult to observe given the kinetics of the process. In this work, the splat formation of glass and alumina is theoretically compared, showing that glass transition and low-thermal conductivity yield a higher ratio between cooling and flattening times, which strongly modifies their spreading behavior. Wipe tests show that splash—splat transition temperature can be modified by the glass composition and its subsequent hydrodynamic properties. The detection of peculiar remaining objects, such as fibers and wavelets shows the possibility of "freezing" some phenomena that are totally unobservable with crystalline oxides, except with high-velocity observations.

Keywords cooling, fragmentation, glass, splat, substrate temperature, wavelets

1. Introduction

In spite of its limited thermo mechanical properties in the as-sprayed conditions (low fracture toughness and hardness, low wear and thermal shock resistance), glass may represent an interesting alternative to crystalline oxides when specific applications are required, such as acid resistant hermetic coatings (Ref 1-5), chemically active coatings (Ref 6-8), and decorative (colored) applications (Ref 9-14). The atmospheric thermal spraying of crystalline oxides (APS, flame spraying) is well known for its inter-splat porosity (Ref 15-16), which explains good thermal properties, as well as the difficulty to obtain dense, hermetic coatings. Low Pressure Plasma Spraying (LPPS) is able to yield more dense coatings (Ref 17), but requires higher investment costs. Moreover, the thermal spraying of pigments and colored single oxides yields a restricted spectrum of colors, due to the alterations of redox and crystalline state during in-flight melting (Ref 18). Glass particles are not able to produce dense as-sprayed coatings, but a thermal post treatment may allow to completely seal the coating (Ref 5, 19) and, sometimes, to produce a glass-ceramic material with improved mechanical properties (Ref 20-21). Composite material can be used to further improve these properties, for example with alumina or yttrium stabilized zirconia (YSZ) (Ref 2, 5, 22-24). Moreover, thermal conductivity of glass is very low (1.2 W/m K, when compared to YSZ: 2.7 W/m K and alumina: 7.4 W/m K (Ref 25-26)), which allows the pigments within glass particles to be hardly heated before impinging onto the substrate, while the glass surface is in liquid or viscoelastic state. In some cases, this effect allows to maintain the original color of the pigment.

This low-thermal conductivity, combined with the glass transition property and a low density, give place to very specific splat formation mechanisms.

The flattening of thermally sprayed crystalline oxides or metallic particles has been widely characterized and modeled (Ref 27-30), as well as the relationship between their hydrodynamic properties (viscosity, surface tension versus temperature) and the spreading factor (ξ = splat diameter/droplet diameter $= a \cdot \mathrm{Re}^b$, see Table 1) and trend to splash ($K = \sqrt{We} \cdot \sqrt{\mathrm{Re}} > 57.7$ (Ref 29)).

However, experimental hydrodynamic information is not always available for molten crystalline oxides, particularly those with a high melting point, which makes it difficult to model the flattening phenomenon. Although the viscosity of slag was successfully modeled (Ref 31) and though alumina (Ref 30) was experimentally characterized, the lack of data led some authors to assume that YSZ has the same behavior as alumina (Ref 32-33). However, Shinoda et al. (Ref 34) yielded an interesting estimation of YSZ viscosity versus temperature by characterizing splat cooling of plasma-sprayed YSZ particles, and assuming that $\xi = 0.83 \cdot \mathrm{Re}^{0,2}$. On the other hand, oxide glass is well understood and modeled: several authors (Ref 35-42) give empiric formulae to estimate viscosity (Vogel-Fulcher-Tamann law) and surface tension versus temperature from their chemical composition by using mixing laws. Their suitability in a wide compositional range helps to predict the processing properties in the glass industry, and could be extended to thermal spraying as well.

Thermal properties are another key aspect to understand the competition between flattening and cooling mechanisms. Though both processes are supposed to be simultaneous (Ref 43), Jones (Ref 44) assumes their sequential character, which allows to calculate the cooling

Thierry Poirier, Grupo de Ingeniería de Superficies, Universidad Simón Bolívar, AA 89000, Caracas 1080ª, Venezuela; and **Marie Pierre Planche**, **Olivier Landemarre**, and **Christian Coddet**, LERMPS, UTBM, Site de Sévenans, 90010, Belfort cedex, France. Contact e-mail: tpoirier@usb.ve.

Nomenclature

a,b	Empirical flattening coefficients, dimensionless
c	Wavelets speed, m/s
Cp	Heat capacity of the particle in the liquid phase, J/kg.K
D	Initial diameter of the particle, m
D_{splat}	Splat diameter, m
e	Flattened film thickness, m
f	Frequency of wavelets, s^{-1}
F	Degree of fragmentation, dimensionless
g	Gravity constant, m/s^2
K	Sommerfeld number, dimensionless
l	Wavelength, m
l_C	Critical wavelength value before obtaining gravitational predominance, m
L	Latent heat of transformation, J/kg
$\mathcal{L}$	Travel distance of wavelets, m
$\dot{m}$	Particles mass flow rate, kg/s
N	Number of impinging particles during t_{transf}
Nu	Nusselt number, dimensionless
P	Probability, dimensionless
Re	Reynolds number, dimensionless
S_{splat}	Surface area of splat, m^2
$S_{exposed}$	Substrate surface area exposed to impinging particles, m^2
T_g	Glass transition temperature, °C
Ts	Substrate temperature, °C
$T_{glazing}$	Typical glazing temperature, °C
$T_{particle}$	Particle temperature, °C
$T_{transformation}$	Change of state temperature, °C
$\mathcal{T}$	Period between wavelets, s
t_{transf}	Cooling time, s
t_{splat}	Flattening time, s
U	Spreading velocity, m/s
V	Particle velocity, m/s
V_i	Volume of a size class of particles, m^3
V_{total}	Total volume of particles, m^3
We	Weber number, dimensionless

Greek symbols

ΔT	Temperature gap between particle and transformation temperatures, °C
ξ	Spreading factor, dimensionless
ρ	Particle density, kg/m^3
λ	Thermal conductivity, W/m K
μ	Particle viscosity, Pa.s
σ	Surface tension, N/m
Ξ	Ratio between cooling and flattening time, dimensionless
Ψ	Feedstock intrinsic prefactor for Ξ and t_{transf}
Ω	Wavelet pulsation, rad/s

Table 1 Values of a and b according to several authors (Ref 28, 29)

a	b	Author
1.2941	0.2	Madejski
1.06	0.125	Ohmori
0.5	0.25	Pasandideh-Fard
1	0.2	Trapaga
0.83	0.2	Yoshida
1.04	0.2	Liu
0.925	0.2	Bertagnolli
1.025	0.2	Li
0.43	0.33	Shinoda

time in an easier way, since impinging droplets would completely flatten (their disk surface depending on initial diameter D and on ξ) before transferring their heat into the substrate. Thus, transformation time of the liquid droplet/disk (solidification onto a cold substrate, in the case of Fukumoto et al. (Ref 45); evaporation onto a hot substrate in the case of Liu et al. (Ref 46)) would be calculated as:

$$t_{transf} = \frac{4\rho \cdot L}{9Nu \cdot \lambda \cdot \Delta T \cdot \xi^4} \cdot D^2 \qquad \text{(Eq 1)}$$

where $Nu = 3.66$ (Ref 46) and $\Delta T = |T_{particle} - T_{transformation}|$. More accuracy would be yielded by replacing L by $(L + Cp\Delta T)$, where Cp is the heat capacity of liquid before its solidification. Therefore, considering $\xi = a \cdot Re^b$, it comes:

$$t_{transf} = \frac{4}{9Nu \cdot a^4} \cdot \frac{\rho^{0.2} \cdot \mu^{0.8} \cdot (L + Cp \cdot \Delta T)}{\lambda \cdot \Delta T} \cdot \frac{D^{(2-4b)}}{V^{4b}} = \Psi \cdot \frac{D^{(2-4b)}}{V^{4b}} \qquad \text{(Eq 2)}$$

Flattening time was estimated by Schiaffino et al. (Ref 47) as $t_{splat} = D/V$ when $We > 1$ and $Re > 1$. Therefore, the ratio between cooling and flattening time would be:

$$\Xi = t_{transf}/t_{splat} = \Psi \cdot (D.V)^{1-4b} \qquad \text{(Eq 3)}$$

The thermal resistance of splat-substrate interface could increase the value of t_{transf}, depending on substrate temperature and on the presence of adsorbates (Ref 48, 49) on its surface. However, assuming similar conditions with respect to this aspect, a comparison of behaviors of impinging droplets of alumina and commercial soda lime silicate container glass can be estimated (Table 2 and Fig. 1). Independently from diameter and velocity, cooling time and value of Ξ of glass particles will be 22 times higher than that of alumina. Therefore, if Jones (Ref 44) hypothesis about sequential flattening and cooling of splats could be questionable for alumina, it appears quite suitable for glasses: this feedstock will remain fluid during a significant lapse of time after flattening. On the other hand, although glass particles are supposed to flatten and splash half as frequently as alumina (Madejski and Sommerfeld prefactors in Table 2 anticipate the intrinsic propensities of both feedstocks), specific phenomena, such as fragmentation, are likely to appear at the edge of the glass splats. Moreover, Li et al. (Ref 50) pointed out that

Table 2 Comparison of flattening and cooling trends of alumina and soda lime silicate glass

Feedstock	Alumina (Ref 26, 30, 53)	Soda lime silicate glass (Ref 7, 25, 35, 41, 54)
ρ (kg/m^3) vs. T (°C)	$2790(1-\alpha \cdot (T-2227))$; $\alpha = 4.22 \cdot 10^{-5}$	$2492(1-3\alpha(T-Tg))$; $\alpha = 1.05 \cdot 10^{-5}$
μ (Pa.s) vs. T (°C)	$2.87 \cdot 10^{-9} \cdot (T+273) \cdot \exp(20500/(T+273)) \approx 4.9 \cdot 10^{-3}$ at 3000 °C	$10^{[0,7843+4609,3/(T-234,96)]} \approx 131 \cdot 10^{-3}$ at 3000 °C
σ (N/m) vs. T (°C)	$0.745-0.00004\ T \approx 0.35$ at 3000 °C	$0.414-0.000021\ T \approx 0.28$ at 3000 °C
λ (W/m K)	7.4	1.2
L (J/kg)	1054000	0
Cp (J/kg.K)	900	600
Madejski prefactor: $(\rho/\mu)^{0.2}$	14	7
Sommerfeld prefactor ($\rho^{0.75}/\mu^{0.5} \cdot \sigma^{0.25}$)	1803	937
Ψ	0.80	17.80

All prefactors are estimated at T = 3000 °C (see experimentation)

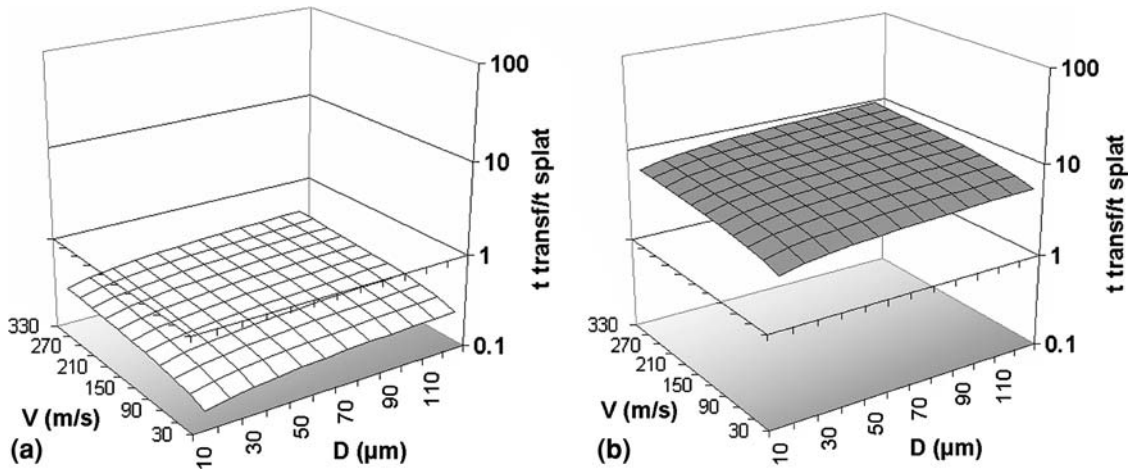

Fig. 1 Estimation of $\Xi = t_{transf}/t_{splat}$ for (a) alumina and (b) soda lime silicate glass particles impinging at T = 3000 °C (see experimentation)

incompletely molten particles that impinge onto a substrate have a higher trend to splash, which should be the case for (thermally insulating) glass particles: Thus, splashed and partly unmolten objects can be predicted for glass, from its comparison with alumina.

2. Experimentation

Several commercial glass frits (see Table 3) were hand crushed and planetary milled by Fritsch pulverisette 6, then sieved (40 µm, granulometry measured by Malvern Mastersizer 2000E) and thermally sprayed by APS (Sulzer Metco F4 torch, Ar-H2: 35-8 slpm, current intensity 500 A, power 18 kW, spraying distance: 100 mm). In-flight temperature and velocity profiles were measured by DPV 2000 (Tecnar Automation, St Bruno, QC, Canada). Particle velocities were measured between 240 and 300 m/s with surface temperatures between 2700 and 3000 °C, depending on their position within the jet. Wipe tests were made in front of AISI 316L polished (0.25 µm) and acetone degreased coupons. A preheating between 170 and 310 °C was performed using hot air and controlled by optical pyrometry (Land Z5365). Glass splats were subsequently observed by optical microscopy (Nikon Epiphot) and Scanning Electron Microscopy (SEM: Jeol 5800LV), and the perimeter and area of each object were determined by image analysis (45-180 objects studied for each case). The equivalent splat perimeter was established from the splat area, and the degree of fragmentation was calculated as follows:

$$F = \text{Actual splat perimeter/Equivalent perimeter} = \text{Actual perimeter}/\sqrt{(4\pi \cdot \text{area})}$$

Schott (zinc-lead borate), Escol and Cerfav T1 (borosilicates) glasses which were considered in this study are not completely characterized with respect to their viscosity: Arrhenius approximations ($\log(\mu) = A + B/T$) are possible near their measured characteristic points at low temperatures, but the whole VTF curve ($\log(\mu) = A + B/(T - T_0)$) cannot be obtained. However, they are potentially more fluid than classical soda lime and Cerfav Z5M (low boron) silicate glass at high temperatures. Lower surface tensions are also expected for those glasses, which then should be more likely to splash.

Table 3 Compositions, granulometry, and hydrodynamic information of the studied glass frits

Composition	Soda lime silicate	Cerfav Z5M	Escol ARB342B	Schott G017-209	Cerfav T1
SiO_2	72.7	70			51.2
B_2O_3	...	2			6.8
Sb_2O_3	...	1			...
Al_2O_3	1	1			1.9
Li_2O	...	...			4.8
Na_2O	14.1	16			10.2
K_2O	...	5			...
CaO	8.1	...			11.4
MgO	4.0	...			4.6
BaO	...	2.5			...
ZnO	...	...	...	...	9.1
d_{10}, μm	5.3	4.2	3.6	4.8	3.4
d_{50}, μm	19.3	18.9	16.7	17.5	18.5
d_{90}, μm	43.4	52.2	50.3	44.8	63.3
Strain point, °C ($\mu = 10^{13.5}$ Pa.s)	485	518	...	...	...
Tg, °C ($\mu = 10^{12}$ Pa.s)	511	547	453 (a)	416	430-500 (b)
Dilatometric softening point, °C ($\mu = 10^{10.3}$ Pa.s)	554 (a)	587	489	439 (a)	
Littleton point, °C ($\mu = 10^{6.6}$ Pa.s)	673	726	591 (a)	499	500-600 (b)
$T_{glazing}$ ($\mu = 10^{2.3}$ Pa.s) (°C)	1088	1140	780	...	...
μ (3000 °C) (Pa.s)	0.131	0.076	...	...	...
σ (3000 °C) (N/m)	0.28	0.30	0.27	0.22	0.24

(a) Arrhenius approximation from commercial data
(b) Extrapolation of Lakatos formula and qualitative comparison with other commercial glasses

3. Results and Discussion

3.1 Flattening and Cooling Behavior

The spreading factor experimental value ξ of the studied objects (Fig. 2) was calculated as the ratio between the median values of splat (D_{splat}) and particle (d_{50}) diameters. Median and maximum values of degree of fragmentation F (Fig. 3) were compared with the typical values of alumina and zirconia, as measured by Bianchi (Ref 51), Shinoda et al. (Ref 52), and Li et al. (Ref 50). Their evolution with substrate temperature shows that spreading and fragmentation occur more easily on cold substrates, whereas preheating yields lower spreading values than that of alumina. However, the splats seem to be more fragmented than classical oxides, particularly for the highly fusible borate glasses with low surface tension. The high calculated value of $\Xi = t_{transf}/t_{splat}$ (Table 4) explains the remaining fluidity of glass after flattening, which allows subsequent fragmentation (flattening splash) that does not occur so easily for YSZ and alumina. At higher temperatures, F appears to be much lower, even for easily fragmented Schott and borosilicate glasses: this could be explained by a better heat transfer onto the substrate (Ref 27). Transition temperatures (splash-splat) of soda lime silicate glass lies under 170 °C, which is comparable with alumina, whereas the other studied glasses seem to keep yielding splashes around 300 °C (Fig. 4).

3.2 Morphology of Splats

Other characteristic aspects of glass splats are visible in Fig. 5-7: unmolten core and peripheral thin film are often observed (see irisation effect in Fig. 5a): This confirms the high-thermal gradient that takes place within glass particles, as studied by Zhang et al. (Ref 3). This gradient was

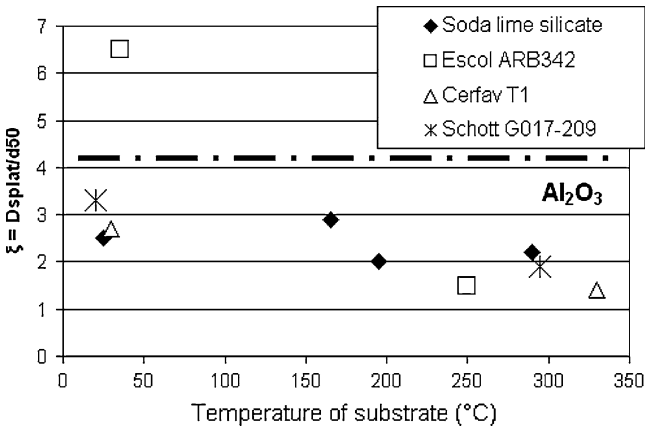

Fig. 2 Spreading factor (ξ) of several glass compositions depending on substrate temperature (T_s), compared with maximum values of alumina splats (after Bianchi (Ref 51))

considered (Ref 50) as a key aspect to predict the high fragmentability of glass splats. The formation of a very thin film is a classical phenomenon at macroscopic scale when excessively fluid glass is blown with too much pressure by a craftsman. Another classical phenomenon, which is seen here at microscopic scale, is the fiberization of the splats, with very long (up to 2 millimeters) fibers (Fig 6a). The observation of such objects usually requires a high velocity camera when crystalline oxides are thermally sprayed (Ref 27). The remaining fluidity after flattening may explain this effect, as well as the beginning of coalescence that is observed between a recently flattened splat and another splat (Fig. 6b). Gawne et al. (Ref 1) report a similar effect at high substrate temperatures with borosilicate glass. This peculiar ''slow freezing'' behavior

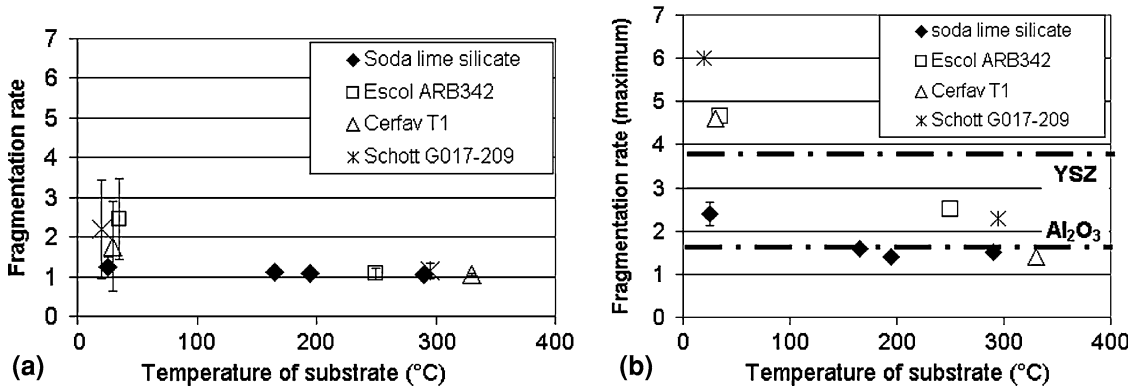

Fig. 3 Degree of fragmentation (F) of several glass compositions depending on substrate temperature (T_s): (a) median value, (b) maximum value, compared with maximum values of alumina (after Escure (Ref 30)) and YSZ (after Li et al. (Ref 50) onto substrates at room temperature)

Table 4 Comparison of estimated cooling and flattening times, for given diameter and velocity conditions

Feedstock	Alumina	Soda lime silicate glass
t_{transf} (ns)	8-158	186-3518
t_{splat} (ns)	33-417	33-417
$\Xi = t_{transf}/t_{splat}$	0.24-0.40	5.3-8.8

of glass splats allows to study *a posteriori* their spreading mechanism, and to identify some effects that would be hardly observable with crystalline oxides.

3.3 Observation of Wavelets in the Glass Splats

3.3.1 Origin of Wavelets. When a splat remains fluid for a long time (i.e., as long as its temperature is above its

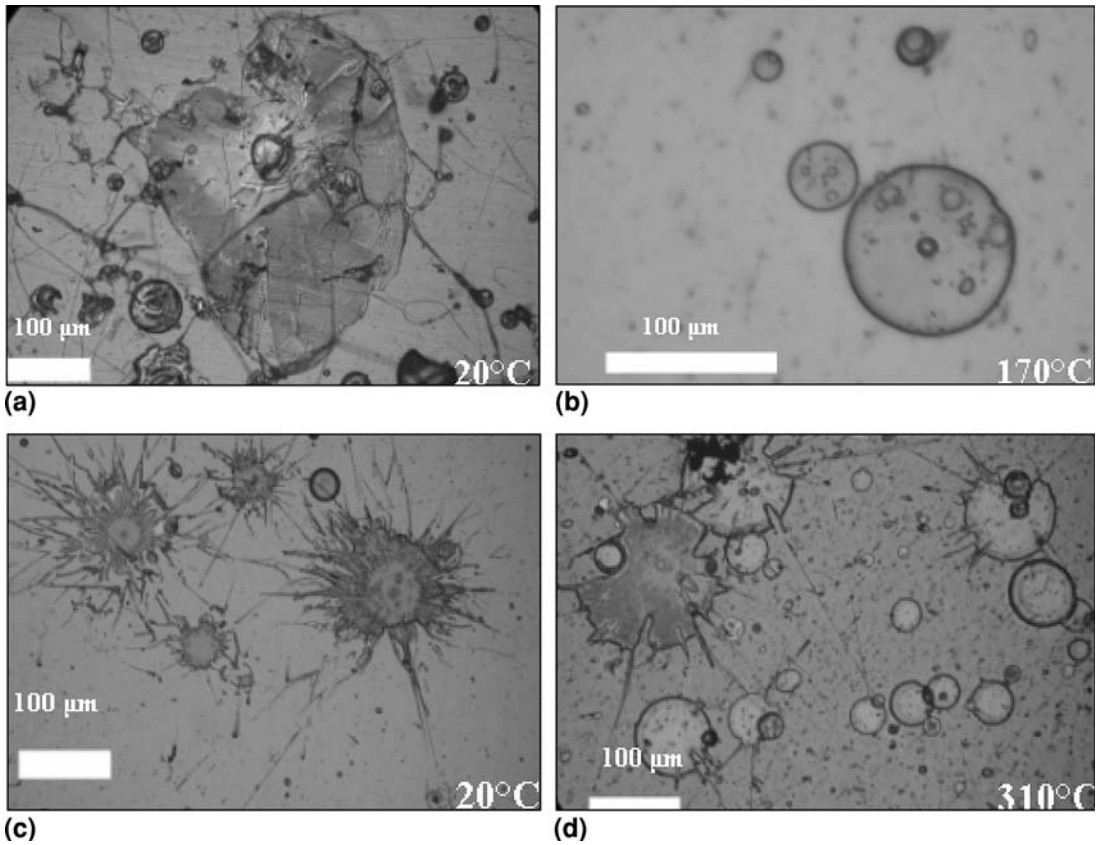

Fig. 4 Aspect of splats of (a, b) soda lime silicate glass and (c, d) Schott G017-209 (Zn-Pb-B) glass with substrate temperatures of (a, c) $T_s = 20$ °C, (b) $T_s = 170$ °C, and (d) $T_s = 310$ °C

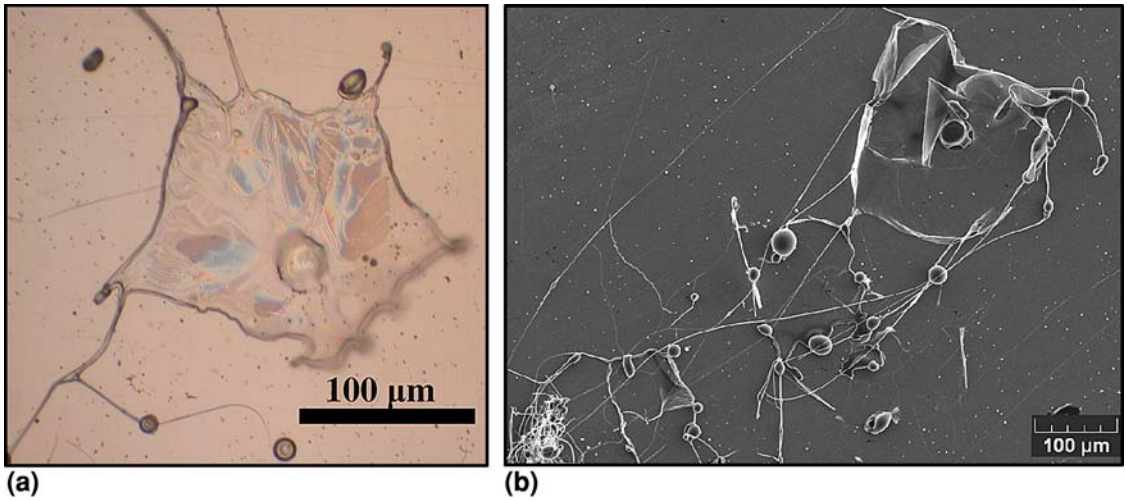

Fig. 5 Unmolten core and peripheric film: here: Cerfav Z5M splat (Ts = 20 °C) seen under optical microscopy (a) and SEM (b)

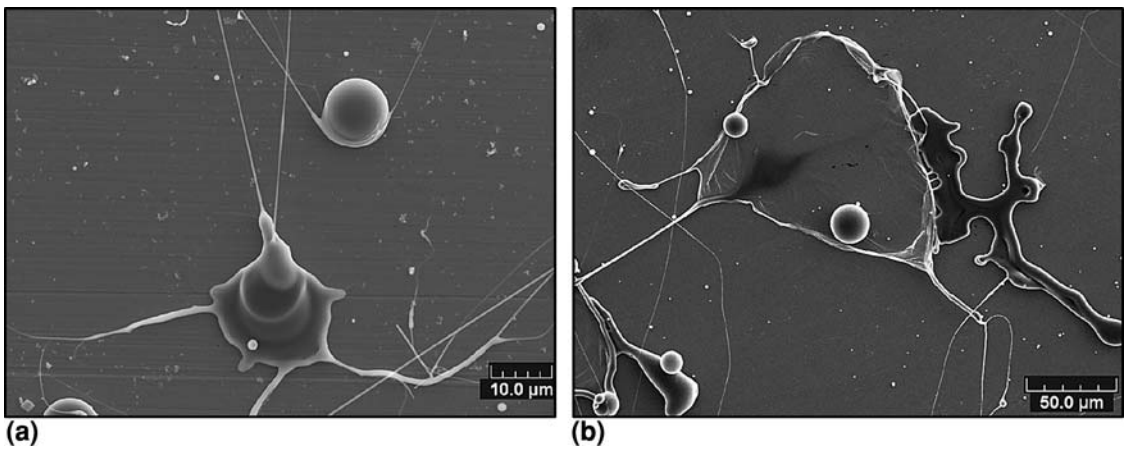

Fig. 6 (a) Fiberization of two objects and (soda lime silicate, $T_s = 20$ °C); (b) beginning coalescence of a recently flattened splat (right) with another splat (left) (Cerfav Z5M, $T_s = 20$ °C)

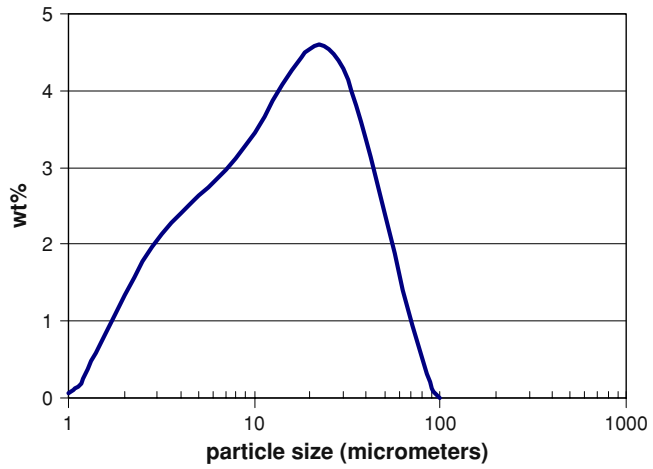

Fig. 7 Size distribution of Z5M glass powder

solidification temperature, T_{fusion}, for a crystalline oxide, Tg for a glass), the probability of the occurrence of a second particle impact at the same location (before the primary splat cools down) becomes not negligible. Of course, the determination of a precise value is quite difficult due to the evolution of splat size with time and also to surfusion aspects (Ref 4). Thus, in order to simplify the probability calculus, splats will be considered in the following as isothermal and fluid splats, which have their final surface area during all the lapse of time t_{transf}. During this lapse of time, a number N of particles will impinge onto a total exposed surface $S_{exposed}$. For this whole surface, the considered splat (surface area S_{splat}) will receive a part of these particles. Each impinging particle has a probability $P_{contact\ 1particle} = S_{splat}/S_{exposed} = 1 - P_{non\text{-}contact}$ of touching the studied splat. Thus, the global non-contact probability is $P_{non\text{-}contact} = [1 - S_{splat}/S_{exposed}]^N$ and the global contact probability is $P_{contact} = 1 - P_{non\text{-}contact}$. The value

of N depends on several factors: (a) the mass particle flow rate $\dot{m}$, (b) the powder volumetric mass, (c) the size distribution (a finer and lighter powder yields a higher value of N): $N = \frac{\dot{m}}{\rho} \cdot t_{transf} \cdot \sum_i \left[\frac{V_i}{V_{total} \frac{\pi}{6} d_i^3} \right]$. For example, a Z5M glass powder (2492 kg/m^3) with the size distribution described in Fig. 7, thermally sprayed with a 2 g/min flow rate over a 100-µm diameter splat ($t_{transf} = 2 \cdot 10^{-6}$ s), corresponds to $N = 700$ particles. If the exposed surface is 2 × 2 cm^2, the contact probability will be 1.4%, i.e., 1 chance out of 70. This means a moderate but quite significant probability of observing this phenomenon. On the other hand, an alumina powder (much shorter cooling time) with the same size distribution and spraying conditions, would have $P_{contact} = 0.06\%$, i.e., 1 chance out of 1700. If commercial alumina (22-45 µm) were used, $P_{contact}$ would decrease to 1 chance out of 200000.

3.3.2 Identification of the Secondary Impact Phenomenon. Some glass splats, such as the one displayed in Fig. 8, show the presence of concentric wavelets. The distance between each wave from their center appear to be increasing, as shown in Fig. 9, and the waves are not visible on their rear front. This situation seems clearly to correspond to the impact of a secondary particle, which impinged onto the spreading splat, as glass was still hot and fluid. The profile of waves leads to conclude that the spreading velocity U of the splat was inferior to the wavelet speed c. The information given by the secondary impact could then supply a better knowledge of the local spreading velocity than the global estimation given by Schiaffino's (Ref 47) model, which suggests a median spreading velocity U = V (here: V = 270-300 m/s) only when c could be accurately estimated.

3.3.3 Estimation of Wavelet Speed. *Kinematical Approach*: the maximum value of c can be calculated as follows: c = l/T, T being the necessary time period to travel through the distance l (≈1.5 µm) between 2 successive wavelets. The observation of SEM picture (Fig 8) shows

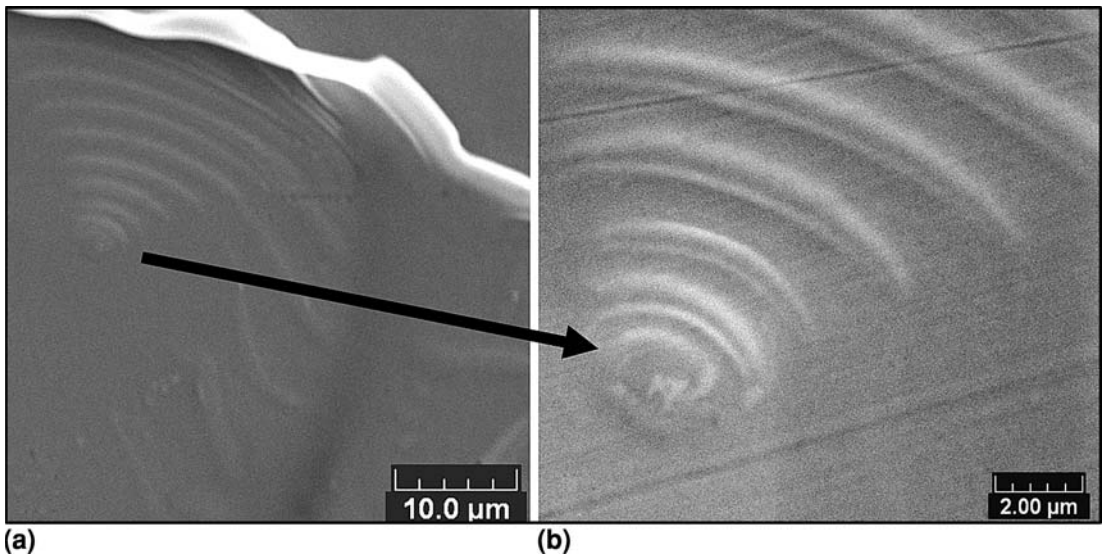

Fig. 8 Wavelets observed by SEM on a Cerfav Z5M splat

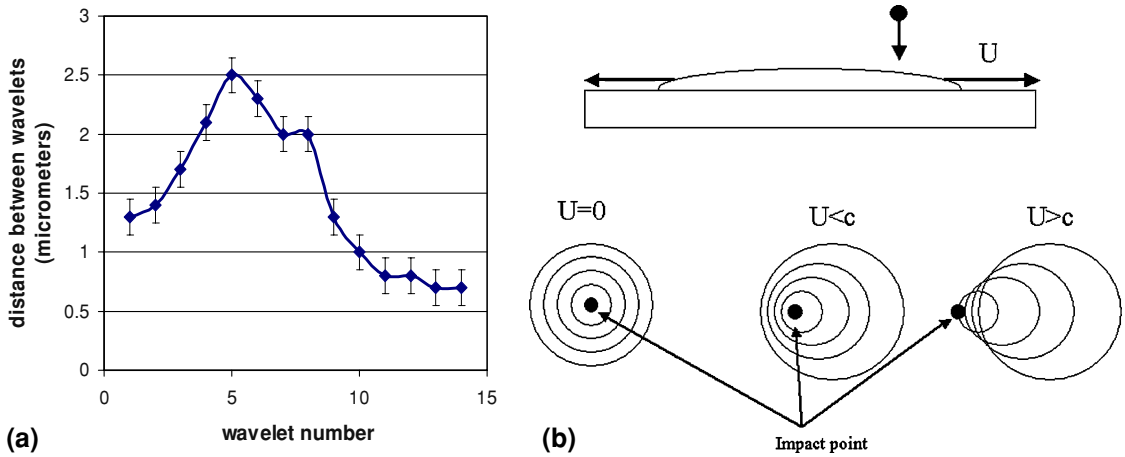

Fig. 9 (a) Distance between wavelets observed by SEM on a Cerfav Z5M splat, (b) identification of the phenomenon: U < c

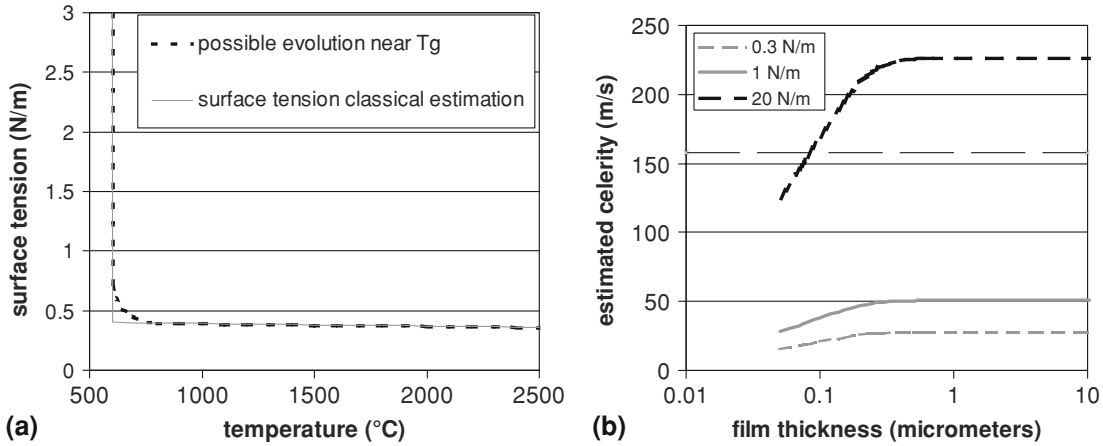

Fig. 10 (a) Suggested evolution of σ(T) near Tg, and (b) subsequent evolution of wavelet speed versus film thickness assuming several values for surface tension

$n = 14$ wavelets, and a total travel distance $\mathcal{L} = 21$ μm ≈ n.l between the impact point and the edge of the splat. It is to note that wavelets 13-14 are visible at the very edge of the splat, and that wavelets 8-14 present a harsh reduction of l, maybe because of a local thickness change. The necessary time to produce all these wavelets should be inferior to the estimated spreading time (t_{splat}), therefore:

$$n \cdot T \leq t_{splat} \text{ thus } T \leq t_{splat}/n \text{ and } c > n \cdot l/t_{splat} \approx \mathcal{L}/t_{splat} = \mathcal{L}/(D/V) = \mathcal{L} \cdot V \cdot \xi / D_{splat} \quad \text{(Eq 4)}$$

giving $c > 21.10^{-6} \times 300 \times 2.5/100.10^{-6} = 158$ m/s. Under this kinematical point of view, the minimum speed can then be estimated. But this does not supply information about the local spreading velocity ($U < c$), which is only supposed to be inferior to the median velocity $U = V$ (Ref 47).

Hydrodynamic Approach: the similarity with the waves produced in a water film (G.B. Homsy, 2007, Personal communication; P. Belleudy, 2007, Personal communication; M. Rabaud, 2007, Personal communication), considering $c = l \cdot f = l \cdot \omega/2\pi$, yields:

$$\Omega = \sqrt{\left(g \cdot \frac{2\pi}{l} + \frac{\sigma}{\rho} \cdot \frac{8\pi^3}{l^3}\right) . \tanh\left(\frac{2\pi . e}{l}\right)} \quad \text{(Eq 5)}$$

where e = film thickness, g = gravity constant.

The first term of the equation corresponds to the gravitational component of the waves, whereas the second term describes the capillary component. The former term is insignificant, since measured value of l (1-2 μm) is very inferior to $l_C = 2\pi\sqrt{(\sigma/(\rho.g))} \approx 21000$ μm. This hypothesis is confirmed by the fact that this impact took place onto a vertical substrate. Thus, the studied phenomenon is strictly capillary. The density and surface tension of the glass are known (see Table 3: σ ≈ 0.3 N/m), therefore the only unknown value necessary to estimate ω would be the value of the film thickness *e* in the glass splat. According to the irisation effects seen in optical microscopy (see Fig. 5a), *e* is expected to have micrometric or submicronic values. An evolution study with 50 nm < *e* < 10 μm yields speed values *c* between 15 and 26 m/s (see Fig. 10). However, this result is much lower than the minimum value estimated by the kinematical approach. This fail of the hydrodynamic approach probably comes from the assumption of a completely isothermal fluid, with a constant and low surface tension. In fact, the surface of the flattening glass splat in contact with air has probably a higher surface tension than the calculated value at 2700-3000 °C. The glass transition phenomenon could allow the existence of a progressive increase of σ(T) near Tg, instead of a first order increase when liquid (finite value σ (T) ≈ 0.3 N/m) acquires a "solid" behavior (σ → ∞). The evolution of the estimated wavelet speed, supposing an external surface temperature near Tg, give values (Fig. 10) that are more compatible with the kinematical approach when the estimated surface tension is above 10 N/m. Thus, the difficulty of measuring the surface tension of glass near Tg makes it difficult to employ the hydrodynamical approach to estimate c. However, it seems to open interesting perspectives about the understanding of the hydrodynamics of glass and splats.

4. Conclusion

Glass transition and low-thermal conductivity allow glasses to cool down very slowly, which gives place to higher spreading and degree of fragmentation than for classical oxides, such as alumina. The predicted trends about splat formation, cooling, and fragmentation are confirmed by experimental results, and the effect of viscosity and surface tension, which can be controlled by choosing suitable glass compositions, allows modifying the splash-splat transition temperature. Peculiar morphological aspects were observed on glass splats, such as fiberization, unmolten core, peripheral thin films and post-splat coalescence. Wavelets caused by a secondary impact onto

a still spreading, fluid splat, were identified. The probability of observing these wavelets was compared between glass and alumina, suggesting that these observations are only possible on glass splats. Thus, thanks to its typical properties, glass allows to ''freeze'' some phenomena that are very difficult to visualize when crystalline oxides are used, and offers opportunities of deepening the knowledge of splat formation. From these observations, two methods to estimate the wave speed were proposed, opening interesting perspectives of calculating minimum velocity of the particle spreading on the substrate, even though better accuracy will be required in the knowledge of surface tension values near glass transition to achieve a suitable calculus.

Acknowledgments

The authors thank Philippe Belleudy at Université Joseph Fourier (Grenoble), George « Bud » Homsy at University of California (Santa Barbara) and Marc Rabaud at Université Paris-Sud (Orsay) for their kind assessment about hydrodynamic aspects of wavelets in splats. Technical help from Pierre Bertrand and Pascale Hoog, and bibliographical help from Martine Coddet are also acknowledged.

References

1. D. Gawne, Y. Bao, and T. Zhang, The Effect of Substrate Temperature on the Adhesion of Plasma Sprayed Borosilicate Glass Coatings, *Thermal Spray. A United Forum for Scientific and Technological Advances,* C. Berndt, Ed., (Indianapolis, IN), ASM International, 1997, p 467-472
2. D. Gawne, Z. Qui, T. Zhang, Y. Bao, and K. Zhang, Abrasive Wear Resistance of Plasma Sprayed Glass-Composite Coatings, *Thermal Spray: Surface Engineering Via Applied Research,* C. Berndt, Ed., (Montreal, Quebec), TSS, DVS and IIW, 2000, p 977-981
3. T. Zhang, Y. Bao, and D.T. Gawne, Process Model of Plasma Enamelling, *J. Eur. Ceram. Soc.*, 2003, **23**, p 1019-1026
4. Y. Bao, T. Zhang, and D. Gawne, Analysis of Residual Stress Generated During Plasma Spraying of Glass Coatings, ITSC 98, Nice, France
5. T. Zhang, Z. Qiu, Y. Bao, D. Gawne, and K. Zhang, Temperature Profiles and Thermal Stress Analysis of Plasma Sprayed Glass-Composite Coatings, *Thermal Spray: Surface Engineering Via Applied Research,* C. Berndt, Ed., (Montreal, Quebec), TSS, DVS and IIW, 2000, p 355-361
6. T.M. Lee, E. Chang, B.C. Wang, and C.Y. Yang, Characteristics of Plasma-Sprayed Bioactive Glass Coatings on Ti-6A1-4V Alloy: An In Vitro Study, *Surf. Coat. Technol.*, 1996, **79**, p 170-177
7. E. Verne, M. Ferraris, A. Ventrella, and L. Paracchini, Sintering, Plasma Spray Deposition of Bioactive Glass-Matrix Composites for Medical Applications, *J. Eur. Cer. Soc.*, 1998, **18**, p 363-372
8. E. Verne, M. Ferraris, C. Jana, and L. Paracchini, Bioverit1 I Base Glass/Ti Particulate Biocomposite: In Situ Vacuum Plasma Spray Deposition, *J. Eur. Cer. Soc.*, 2000, **20**, p 473-479
9. G.Z. Komskii and G. Saakov, *Forming Decorative Protective Coatings by Plasma Spraying*, Steklo I keramika no. 4, p 22-24, Izdatel'stvo Lad'ia, Moscow, Russia, April 1991
10. V.S. Bessmertnyi, V.P. Krokhin, V.A. Panasenko, N.A. Drizhd, P.S. Dyumina, and O.M. Kolchina, Plasma Rod Decorating of Household Glass, *Glass Ceram.*, 2001, **58**, p 214-215
11. J. Tikkanen, M. Eerola, and M. Rajala, Coating Glass by Flame Spraying, *J. Non-Cryst. Solids*, 1994, **178**, p 220-226
12. G. Bolelli, V. Cannillo, and L. Lusvarghi, Plasma-Sprayed Glass-Ceramic Coatings on Ceramic Tiles: Microstructure, Chemical Resistance, Mechanical Properties, *J. Eur. Cer. Soc.*, 2005, **25**, p 1835-1853
13. G. Bolelli, L. Lusvarghi, T. Manfredini, and C. Siligardi, Influence of the Manufacturing Process on the Crystallization Behaviour of CZS Glass System, *J. Non-Cryst. Solids*, 2005, **351**, p 2537-2546
14. T. Valente, C. Bartulli, and A. Loreto, Plasma Sprayed Nanostructured Glass Ceramic Matrix Composite Coatings from the CaO-SiO2-ZrO2 Eutectic System, ITSC 2004, Osaka, 10-12/05/2004
15. S.H. Leigh and C. Berndt, Quantitative Evaluation of Void Distributions Within a Plasma-Sprayed Ceramic, *J. Am. Ceram*, 1999, **82**, p 17-21
16. S. Deshpande, A. Kulkarni, S. Sampath, and H. Herman, Application of Image Analysis for Characterization of Porosity in Thermal Spray Coatings and Correlation with Small Angle Neutron Scattering, *Surf. Coat. Technol.*, 2004, **187**, p 6-16
17. A. Refke, D. Hawley, J. Doesburg, and R.K. Schmid, LPPS Thin Film Technology for the Application of TBC Systems, *ITSC 2005*, E. Lugscheider, Ed., May 2-4, 2005, Basel, Switzerland, 6 pages
18. V.S. Bessmertnyi, N.I. Min'ko, V.N. Glaz, P.S. Dyumina, V.P. Krokhin, and M.A. Trubitsin, The Effect of Argon Plasma on Reduction of Variable-Valence Oxides in Synthesis of Minerals, *Glass Ceram.*, 2004, **61**(1-2), p 63-64
19. S. Dallaire, B. Arsenault, and A. De Santis, Investigation of Plasma Sprayed Coatings for Bonding Glass to Metal in Hermetic Seal Applications, *Surf. Coat. Technol.*, 1992, **53**, p 129-135
20. G. Bolelli, L. Lusvarghi, T. Manfredini, and C. Siligardi, Influence of the Manufacturing Process on the Crystallization Behaviour of CZS Glass System, *J. Non-Cryst. Solids*, 2005, **351**, p 2537-2546
21. G. Bayrak and S. Yilmaz, Crystallization Kinetics of Plasma Sprayed Basalt Coatings, *Ceram. Int.*, 2006, **32**, p 441-446
22. G. Bolelli, V. Canillo, L. Lusvarghi, and T. Manfredini, Glass-Alumina Composite Coatings by Plasma Spraying. Part I: Microstructural and Mechanical Characterization, *Surf. Coat. Technol.*, 2006, **201**, p 458-473
23. G. Bolelli, V. Canillo, L. Lusvarghi, T. Manfredini, and M. Montorsi, Glass-Alumina Composite Coatings by Plasma Spraying. Part II: Microstructure-Based Modeling of Mechanical Properties, *Surf. Coat. Technol.*, 2006, **201**, p 474-486
24. V. Cannillo, T. Manfredini, M. Montorsi, C. Siligardi, and A. Sola, Microstructure-Based Modelling and Experimental Investigation of Crack Propagation in Glass-Alumina Functionally Graded Materials, *J. Eur. Cer. Soc.*, 2006, **26**, p 3067-3073
25. H. Zhang, X.Y. Wang, L.L. Zheng, and X.Y. Jiang, Studies of Splat Morphology and Rapid Solidification During Thermal Spraying, *Int. J. Heat Mass Trans.*, 2001, **44**, p 4579-4592
26. D.R. Lide, Ed., *CRC Handbook of Chemistry and Physics*, CRC press, London, 1995, p 12-182
27. P. Fauchais, M. Fukumoto, A. Vardelle, and M. Vardelle, Knowledge Concerning Splat Formation: An Invited Review, *JTST*, 2004, **13**(3), p 337-357
28. C.J. Li, H. Liao, P. Gougeon, G. Montavon, and C. Coddet, Experimental Determination of the Relationship Between Flattening Degree and Reynolds Number for Spray Molten Droplets, *Surf. Coat. Technol.*, 2005, **191**, p 375-383
29. K. Shinoda, T. Koseki, and T. Yoshida, Influence of Impact Parameters of Zirconia Droplets on Splat Formation and Morphology in Plasma Spraying, *J. Appl. Phys.*, 2006, 100(7), Art. No. 074903
30. C. Escure, ''Impact Study of Liquid Alumina Droplets onto a Hot Substrate or a Liquid Alumina Film,'' Ph.D. Thesis, Université de Limoges, November 2000, 55-2000 (in french)
31. G.J. Browning, G.W. Bryant, H.J. Hurst, J.A. Lucas, and T.F. Wall, An Empirical Method for the Prediction of Coal Ash Slag Viscosity, *Energy Fuels*, 2003, **17**, p 731-737
32. M. Vardelle, A. Vardelle, A.C. Léger, and P. Fauchais, Dynamics of Splat Formation and Solidification in Thermal Spraying

Processes, *Proceedings of the 7th NTSC*, 20-24/06/1994, Boston, MS, p 555-562
33. C. Kang and H. Ng, Splat Morphology and Spreading Behavior due to Oblique Impact of Droplets onto Substrates in Plasma Spray Coating Process, *Surf. Coat. Technol.*, 2006, **200**, p 5462-5477
34. K. Shinoda, Y. Kojima, and T. Yoshida, In Situ Measurement System for Deformation and Solidification Phenomena of Yttria-Stabilized Zirconia Droplets Impinging on Quartz Glass Substrate Under Plasma Spraying Conditions, *J. Therm. Spray Technol.*, 2005, **14**(4), p 511-517
35. T. Lakatos, Viscosity-Temperature Relations in Glasses Composed of SiO2-Al2O3-Na2O-K2O-Li2O-CaO-MgO-BaO-ZnO-PbO-B2O3, *Glastecknisk Tidskrift*, 1976, **31**(3), p 51-54
36. T. Lakatos, The Effect of Some Glass Components on the Viscosity of Glass, *Glastecknisk Tidskrift*, 1972, **27**(2), p 25-28
37. E. Tillotson, On the Surface Tension of Silicate and Borosilicate Glasses, *J. Ind. Eng. Chem.*, 1912, **4**(9), p 651-652
38. A.G. Clare, D. Wing, L.E. Jones, and A. Kucuk, Density and Surface Tension of Borate Containing Silicate Glass Melts, *Glass Technol.—Eur. J. Glass Sci. Technol. Part A*, 2003, **44**(2), p 59-62
39. X. Shi, Q. Wang, X. Niu, C. Li, and K. Lu, An Examination of Surface Tension of Binary Lithium Borate Melts as a Function of Composition and Temperature, *JACS*, 2006, **89**(10), p 3222-3228
40. W.D. Kingery, H. Bowen, and D.R. Uhlmann, Introduction to Ceramics. John Wiley & sons, New York, 1960, p 284
41. T. Seward, *Modeling of Glass Making Processes for Improved Efficiency: Final Report*, DE-FG07-96EE41262, 2003
42. A. Priven, General Method for Calculating the Properties of Oxide Glass Forming Melts from Their Composition and Temperature, *Glass Technol.*, 2004, **45**(6), p 244-54
43. B. Dussoubs, A. Vardelle, D. Gobin, and P. Fauchais, Solidification and Cooling of a Plasma Sprayed Droplet: Determination of Cooling Velocity, *Journée SFT'95*, Société Française de Thermique, Limoges, France, p 361-366 (in French)
44. H. Jones, Cooling, Freezing and Substrate Impact of Droplets Formed by Rotary Atomization, *J. Phys. D Appl. Phys.*, 1971, **4**, p 1657
45. M. Fukumoto, S. Katoh, and I. Okane, Splat Behaviour of Plasma Sprayed Particles on Flat Substrate, *Thermal Spraying: Current Status and Future Trends*, A. Ohmori, Ed., High Temperature Society of Japan, Kobe, Japan, 1995, vol. 1, p 353-358
46. Z. Liu and R. Reitz, Modelling Fuel Spray Impingement and Heat Transfer Between Spray and Wall in Direct Injection Diesel Engines, *Numer. Heat Transfer, Part A*, 1995, **28**, p 515-529
47. S. Schiaffino and A. Sonin, Molten Droplet Deposition and Solidification at Low Weber Numbers, *Phys. Fluids*, 1997, **9**(11), p 3172-3187
48. X. Jiang, Y. Wan, H. Hermann, and S. Sampath, Role of Condensates and Adsorbates on Substrate Surface on Fragmentation of Impinging Molten Droplets During Thermal Spraying, *Thin Solid Films*, 2001, **385**, p 132
49. A. McDonald, M. Lamontagne, C. Moreau, and S. Chandra, Impact of Plasma-Sprayed Metal Particles on Hot and Cold Glass Surfaces, *Thin Solid Films*, 2006, **514**(1-2), p 212-222
50. L. Li, A. Vaidya, S. Sampath, H. Xiong, and L. Zheng, Particle Characterization and Splat Formation of Plasma Sprayed Zirconia, *JTST*, 2006, **15**(1), p 97-105
51. L. Bianchi, ''Projection ar plasma d'arc et plasma inductif de dépôts céramiques: mécanisme de formation de la premièrecouche et relation avec les propriétés mécaniques des dépôts'', Ph.D. Thesis, Université de Limoges, January 1995, p 41-1995 (in French)
52. K. Shinoda, A. Yamada, M. Kambara, Y. Kojima, and T. Yoshida, Deformation of Alumina Droplets on Micro-Patterned Substrates Under Plasma Spraying Conditions, *J. Therm. Spray Technol.*, 2007, **16**, p 300-305
53. A. Navrotsky, Thermodynamic Properties of Minerals, *Mineral Physics and Crystallography: A Handbook of Physical Constants*, American Geophysical Union, Washington, DC, 1995, p 18-28
54. A. Kucuk, A.G. Clare, and L.E. Jones, Differences Between the Surface and Bulk of Glass Melts. Part 2. Influence of Redox Ratio on the Surface Properties of Silicate Melts, *Phys. Chem. Glasses—Eur. J. Glass Sci. Technol. Part B*, 2000, **41**(2), p 75-80